blood®
Regular Article

THROMBOSIS AND HEMOSTASIS

Factor VIII exhibits chaperone-dependent and glucose-regulated reversible amyloid formation in the endoplasmic reticulum

Juthakorn Poothong,[1,*] Anita Pottekat,[1,*] Marina Siirin,[1] Alexandre Rosa Campos,[2] Adrienne W. Paton,[3] James C. Paton,[3] Jacqueline Lagunas-Acosta,[1] Zhouji Chen,[1] Mark Swift,[4] Niels Volkmann,[4] Dorit Hanein,[4] Jing Yong,[1] and Randal J. Kaufman[1]

[1]Degenerative Diseases Program and [2]Proteomics Core Facility, Sanford Burnham Prebys (SBP) Medical Discovery Institute, La Jolla, CA; [3]Research Centre for Infectious Diseases, Department of Molecular and Biomedical Science, University of Adelaide, Adelaide, SA, Australia; and [4]Immunity and Pathogenesis Program, SBP Medical Discovery Institute, La Jolla, CA

KEY POINTS

- **In the ER, FVIII forms amyloid aggregates that are dissolved in a chaperone- and glucose-dependent manner to produce secreted functional FVIII.**
- **A short amino acid motif in the A1 domain seeds β-sheet polymerization; binding of ER chaperone BiP to this motif prevents aggregation.**

Hemophilia A, an X-linked bleeding disorder caused by deficiency of factor VIII (FVIII), is treated by protein replacement. Unfortunately, this regimen is costly due to the expense of producing recombinant FVIII as a consequence of its low-level secretion from mammalian host cells. FVIII expression activates the endoplasmic reticulum (ER) stress response, causes oxidative stress, and induces apoptosis. Importantly, little is known about the factors that cause protein misfolding and aggregation in metazoans. Here, we identified intrinsic and extrinsic factors that cause FVIII to form aggregates. We show that FVIII forms amyloid-like fibrils within the ER lumen upon increased FVIII synthesis or inhibition of glucose metabolism. Significantly, FVIII amyloids can be dissolved upon restoration of glucose metabolism to produce functional secreted FVIII. Two ER chaperone families and their cochaperones, immunoglobulin binding protein (BiP) and calnexin/calreticulin, promote FVIII solubility in the ER, where the former is also required for disaggregation. A short aggregation motif in the FVIII A1 domain (termed Aggron) is necessary and sufficient to seed β-sheet polymerization, and BiP binding to this Aggron prevents amyloidogenesis. Our findings provide novel insight into mechanisms that limit FVIII secretion and ER protein aggregation in general and have implication for ongoing hemophilia A gene-therapy clinical trials. (*Blood*. 2020;135(21):1899-1911)

Introduction

Hemophilia A (HA), an X-chromosome–linked bleeding disorder affecting ~10 000 males in the United States, results from deficiency in coagulation FVIII, a component of the intrinsic blood-clotting cascade[1,2] presently treated by protein replacement. Although development of recombinant-derived factor VIII (FVIII) significantly decreased risk of adventitious viral contamination, it greatly increased the cost of treatment, partially due to the low level of FVIII secretion from recombinant mammalian host cells.[3] FVIII is synthesized and translocated into the endoplasmic reticulum (ER) lumen where only properly folded proteins traffic to the Golgi compartment. The accumulation of unfolded/misfolded proteins in the ER activates the unfolded protein response (UPR), an adaptive signaling pathway evolved to resolve ER protein misfolding.[4-6] FVIII is susceptible to misfolding in the ER and was the first native endogenous protein shown to activate the UPR by binding to the ER protein chaperone immunoglobulin binding protein (BiP)/GRP78.[7,8] FVIII expression and an unresolved UPR lead to apoptosis.[9] A comprehensive understanding of the factors required for FVIII folding and secretion is unknown.

FVIII has the domain structure A1-A2-B-A3-C1-C2, where the B domain contains 18 potential *N*-linked glycosylation sites.[1] The A domains have amino acid homology to clotting factor V (FV) and ceruloplasmin, and structural homology to double β-barrel proteins, resembling the fold of cupredoxin domains.[10,11] Energy depletion, with inhibitors of mitochondrial oxidative phosphorylation and glycolysis, selectively inhibits FVIII anterograde trafficking in the early secretory pathway,[12,13] without affecting the trafficking of other proteins, including the homologous clotting FV and von Willebrand factor, even within the same cell.[12,14] A portion of FVIII traffics to the Golgi apparatus for processing by Furin to produce a heterodimer composed of an amino-terminal ~200-kDa heavily glycosylated heavy chain (HC; A1-A2-B) in complex with a carboxy-terminal ~80-kDa light chain (LC; A3-C1-C2) linked through 2 copper ions in each of the A1 and A3 domains[15] that probably stabilize the A1 and A3

domains to promote A1-A3 interaction.[16,17] Unfortunately, the molecular basis of FVIII folding and trafficking through the secretory pathway is poorly defined. Here, we demonstrate that FVIII forms amyloid-like structures in the ER that can disaggregate and refold, and be secreted as functional FVIII in mammalian cells. In addition: (1) a short amino acid motif, which we termed Aggron, in FVIII is necessary and sufficient to seed aggregation; (2) glucose (Glc) metabolism is required to maintain FVIII solubility; and (3) 2 chaperone families, calnexin (CANX)/calreticulin (CRT) and BiP, promote solubility, the latter of which is also required for FVIII disaggregation by interaction with Aggron.

Materials and methods

Cell lines

Parental Chinese hamster ovary cells (CHO-K1) and 2 CHO-K1 clones were engineered for constitutive FVIII expression (10A1),[8] or, for inducible FVIII expression (H9),[18] were previously described. COS-1 (ATCC CRL-1650), 293T (ATCC CRL-3216), and HepG2 (ATCC HB-8065) were obtained from the American Type Culture Collection (ATCC).

Reagents

All reagents are specified in supplemental Methods (available on the *Blood* Web site).

Standard methods

Plasmid construction and treatment with metabolic inhibitors[19] are detailed in supplemental Methods. FVIII immunohistochemistry, activity and antigen measurement, pulse-chase and immunoprecipitation (IP) analyses,[18] co-IPs and western blotting, sucrose gradient sedimentation,[19] and membrane filtration[20] were standard as detailed in supplemental Methods.

Immunogold-labeling transmission electron microscopy

CHO-K1 or suberoylanilidehydroxamic acid (SAHA)-treated H9 cells were processed for immunogold localization of FVIII as in supplemental Methods.

Negative-stain TEM and transmission cryo-EM

Lysates from CHO-K1 or sodium butyrate (NaB)-treated H9 cells were subjected to sucrose gradient sedimentation for FVIII IP, elution, and analysis by transmission electron microscopy (TEM) and transmission electron cryomicroscopy (cryo-EM) as in supplemental Methods.

Quantification and statistical analysis

All statistical analysis used Prism software 7. *P* values were calculated using 1-way analysis of variance (ANOVA). $P < .05$ was considered significant. Statistical significance in figures and legends is denoted by asterisks (***$P < .001$; ****$P < .0001$).

Results

FVIII forms amyloid-like aggregates in the ER

We studied FVIII secretion in 2 stable CHO cell clones engineered to express human FVIII. 10A1 cells constitutively express high levels of FVIII without UPR activation.[18] In contrast, H9 cells express a low level of FVIII that is inducible by histone deacetylase inhibitors (NaB or SAHA) that is coupled with UPR activation. In H9 cells, NaB treatment increased FVIII expression over time and activated UPR and apoptosis (Figure 1A).[8,19] Previous studies using sucrose gradient sedimentation demonstrated newly synthesized FVIII transiently aggregates in CHO cells.[19] To measure FVIII aggregation in a more reproducible, robust, and convenient manner, we used filtration through cellulose acetate (CA) membranes, which selectively retains amyloid aggregates.[20] CA retention was normalized to the total amount of FVIII determined by western blotting or by retention on nitrocellulose (NC) membranes, which bind all cell proteins. FVIII aggregation occurred upon increased FVIII synthesis (supplemental Figure 1A-B) and inversely correlated with the level of FVIII secretion (supplemental Figure 1C). Immunofluorescence microscopy demonstrated similar diffuse ER localization of FVIII in H9 and 10A1 cells characterized by colocalization with KDEL-containing ER proteins (Figure 1Bi; supplemental Figure 2i). NaB induction of FVIII synthesis in H9 cells increased FVIII staining that also colocalized with the KDEL ER marker (Figure 1Bii), suggesting that ER retention occurs upon increased synthesis. Energy depletion, with inhibitors of mitochondrial oxidative phosphorylation and glycolysis, causes FVIII aggregation and selectively inhibits FVIII trafficking to the Golgi.[12,14] Treatment of 10A1 cells or H9 cells with 2′-deoxyglucose (2DG), an inhibitor of glycolysis, and sodium azide (NaN_3), an inhibitor of oxidative phosphorylation, to deplete cellular energy caused FVIII and KDEL-containing ER proteins to colocalize to large perinuclear structures (Figure 1Biii; supplemental Figure 2i vs ii). Thioflavin-S (Thio-S) selectively binds β-rich structures such as amyloid and increases fluorescence intensity.[21,22] Intriguingly, 2DG and NaN_3 caused colocalization of Thio-S staining with FVIII, suggesting that FVIII in the ER has amyloid-like properties, especially upon metabolic collapse. Surprisingly, upon replacing the metabolic inhibitors with Glc-containing media for 4 hours, FVIII and KDEL proteins resumed their diffuse web-like ER colocalization, and Thio-S costaining was significantly reduced in both H9 and 10A1 cell lines (Figure 1Biv; supplemental Figure 2iii), suggesting at the morphological level that FVIII aggregates disappear and may traffic the secretory pathway.

FVIII aggregation was also analyzed by immunogold TEM. There was insignificant FVIII reactivity in H9 cells not treated with primary antibody (Figure 1Ci), CHO-K1 cells that do not express FVIII (Figure 1Civ), and modest reactivity in H9 cells that were not induced to express FVIII with SAHA (Figure 1Cii,v). Upon FVIII induction by SAHA in H9 cells, FVIII was detected in clusters detected by 2 independent FVIII antibodies coupled to 12-nm gold particles (Figure 1Ciii,vi). In addition, immunolocalization of PDIA6 by secondary antibody conjugated to 18-nm gold particles demonstrated colocalization and clustering of FVIII and an ER-resident protein (Figure 1Ciii,vi [and magnified to the right of the subpanels]).

The structure of purified FVIII aggregates in NaB-treated H9 cells was analyzed by conventional TEM and transmission cryo-EM. After FVIII induction, H9 cell lysates were sedimented on sucrose gradients.[19] FVIII was immunoprecipitated from each fraction, eluted from the beads, and analyzed by TEM and cryo-EM. Fibrils of ~5-nm diameter were visible in negatively stained TEM images from the heavy-molecular-weight (HMW) sucrose gradient fractions (Figure 1D white arrows) from NaB-treated H9 cells, presumably representing aggregated FVIII. These fibrils

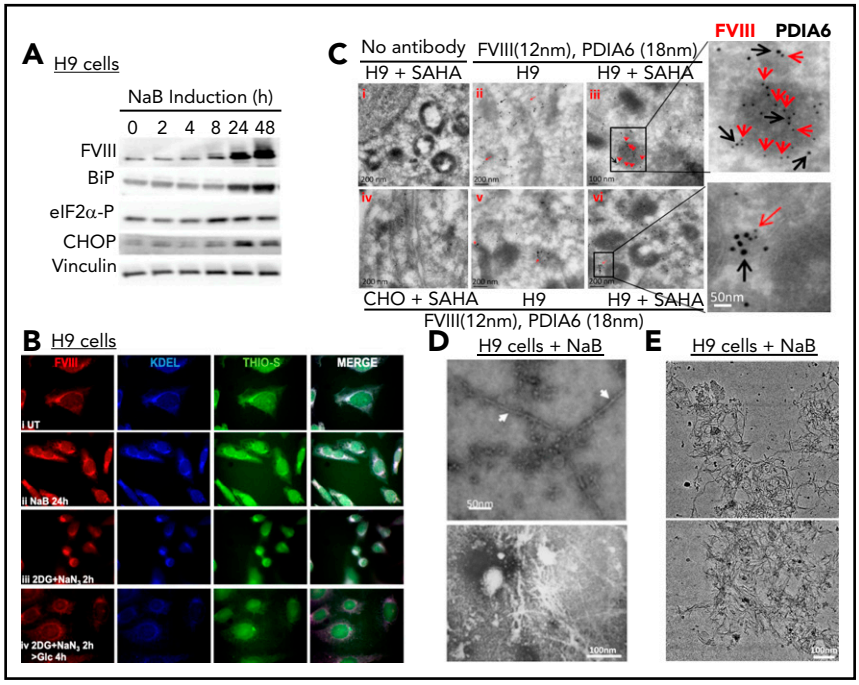

Figure 1. FVIII forms amyloid-like fibrils in the ER. (A) Increased FVIII synthesis activates the UPR. H9 cells were treated with 5 mM NaB for increasing times to induce FVIII expression and cell lysates prepared for immunoblotting with indicated antibodies. (B) FVIII aggregates within the ER lumen. H9 cells were cultured in: (i) complete media; (ii) NaB (5 mM) for 24 hours; (iii) Glc-free media containing 20 mM 2DG and 10 mM NaN_3 for 2 hours; or (iv) 2DG and NaN_3 treatment of 2 hours and then recovered in Glc-containing media for 4 hours. Cells were fixed and stained with Thio-S (green) or antibodies for FVIII (red) and KDEL (blue); original magnification ×40. (C) FVIII colocalizes with PDIA6. CHO-K1 cells and H9 cells were treated without/with 5 μM SAHA for 24 hours, and ultrathin sections were prepared for immunogold labeling and TEM by first staining with FVIII primary antibody using secondary antibody coupled to 12-nm gold particles. Subsequently, grids were stained with PDIA6 antibody using a secondary coupled to 18-nm gold particles: (i) SAHA-treated H9 cells stained without primary antibody; (ii, v) untreated H9 cells; (iii, vi) SAHA-treated H9 cells (insets [panels on the right] show regions in subpanels iii and vi in greater detail; scale bars, iii and vi, 50 nm); and (iv) SAHA-treated control CHO cells. Red and black arrows indicate FVIII and PDIA6 particles, respectively. Scale bars: i, ii, iv-vi: 200 nm; iii, 100 nm. (D-E) FVIII forms amyloid fibrils. H9 cells were treated with 5 mM NaB for 24 hours; lysates were prepared and analyzed by sucrose gradient sedimentation. FVIII in each fraction was immunoprecipitated with FVIII-monoclonal antibody-conjugated Sepharose beads. After IP, FVIII was eluted and analyzed by negative-stain TEM (D) and cryo-EM (E). Two images are shown for each. (D) Arrows indicate FVIII fibrils in the HMW sucrose fractions. Scale bars: top, 50 nm; bottom, 100 nm. (E) Cryo-EM images of FVIII reveal dense networks composed of ~5-nm wide fibrils. Scale bar, 100 nm. CHOP, C/EBP homologous protein; eIF2α-P, phosphorylated eukaryotic initiation factor 2 α subunit; UT, untreated.

were absent in FVIII similarly isolated from the light fractions, which would contain monomeric FVIII (not shown). Cryo-EM images of FVIII immunoprecipitated from HMW fractions displayed dense networks of fibrils with diameters of 5.1 ± 0.5 nm. The fibrils appeared to interact with each other in various ways and form amyloid-like aggregates reminiscent of Poly-Q aggregates observed by cryo-EM in mammalian cells[23] (Figure 1E). Antibody gold labeling for FVIII further confirmed that these fibrils are composed of FVIII. Importantly, no fibrils were detected in fractions similarly prepared from H9 cells that were not induced for FVIII expression (supplemental Figure 3). Therefore, FVIII forms fibrils that are morphologically similar to those reported for other amyloidogenic proteins.[24-26]

Aggregated FVIII disassembles and refolds into secreted functional protein

To examine the fate of FVIII aggregates in cells upon bioenergetic collapse and recovery in Glc, we analyzed aggregation by radiolabel pulse-chase experiments and filtration on CA and NC membranes. Recombinant FVIII (rFVIII) was filtered as a control for properly folded FVIII and did not bind CA membranes (supplemental Figure 4A). 2DG and NaN_3 treatment decreased cellular adenosine triphosphate (ATP) in H9 cells by approximately fivefold (supplemental Figure 4B), and increased FVIII retention on CA membranes (supplemental Figure 4A) in H9 and 10A1 cells, which subsequently declined upon Glc recovery for 4 hours (supplemental Figure 4C). Treatment with autophagy inhibitor 3-methyladenine or proteasome inhibitor Velcade did not stabilize aggregates upon Glc repletion (supplemental Figure 4C), suggesting that these processes do not significantly contribute to eliminating the aggregates. 10A1 cells were pulse-labeled for 20 minutes, chased in unlabeled medium for 20 minutes, and then treated with or without 2DG and NaN_3 for 2 hours. After 2 hours, the cells were recovered in Glc-containing medium for up to 4 hours. Cell lysates and conditioned media were analyzed by FVIII IP, sodium dodecyl sulfate–polyacrylamide gel electrophoresis (SDS-PAGE), and autoradiography. The same lysates were also filtered through CA and NC membranes, which demonstrated aggregation after 2DG and NaN_3 treatment and subsequent resolution upon Glc recovery from 1 to 4 hours (Figure 2Ai). The pulse-chase demonstrated that untreated 10A1 cells efficiently secreted FVIII at 4 hours after the pulse label (Figure 2Aii lanes 1-3). In contrast, 2DG and NaN_3 treatment prevented secretion of the pulse-labeled FVIII (Figure 2Aii lane 4). Upon Glc repletion, labeled FVIII appeared in the medium from 1 to 4 hours (Figure 2Aii lanes 5-8). The total amount of labeled FVIII secreted after 4 hours closely approximated that secreted from cells not treated with 2DG and NaN_3 (100% vs 87%). Notably, recovery in Glc not only increased FVIII secretion (Figure 2Aii lane 8), but also functional FVIII activity in the medium (Figure 2Aiii). Addition of cycloheximide (CHX) to inhibit new protein synthesis during the chase recovery reduced

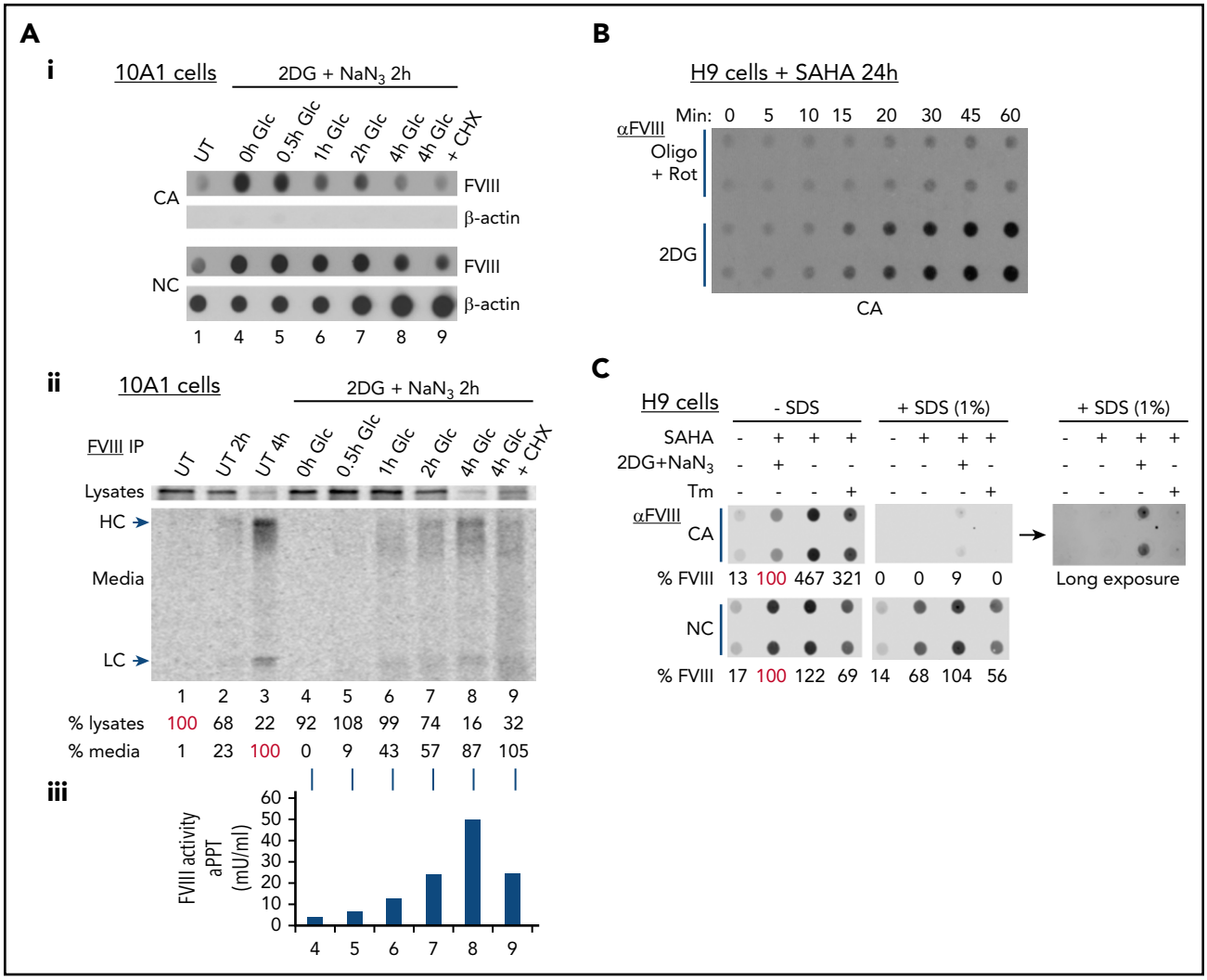

Figure 2. FVIII aggregation is reversible upon restoration of Glc metabolism. (A) FVIII aggregates disassociate and refold into functional secreted FVIII. (i-iii) Kinetics of FVIII aggregation and disaggregation upon altered Glc metabolism was characterized by simultaneous membrane filtration, pulse-chase analysis, and measurement of secreted FVIII activity. (i-iii) The corresponding lane numbers are indicated below the image. 10A1 cells were pulse-labeled for 20 minutes with [^{35}S]-Met/Cys and then chased for 20 minutes with media containing excess-unlabeled Met/Cys to compete synthesis of nascent chains (lane 1). Radiolabeled cells were then fed with complete media for indicated times (ii, lanes 2-3) or Glc-free media containing 20 mM 2DG and 10 mM NaN_3 for 2 hours (i-ii, lanes 4-9). Radiolabeled [^{35}S]-Met/Cys cell lysates and media were harvested after 2 hours (lane 4) or allowed to recover in complete media (5 mM Glc) from 30 minutes to 4 hours (lanes 5-8), or complete media with 10 μg/mL CHX (lane 9). (i) At the indicated times, cell lysates were analyzed by filtration on CA and NC membranes and probed with FVIII and β-actin antibodies. (ii) FVIII was immunoprecipitated from cell lysates and media for analysis by SDS–polyacrylamide gel electrophoresis and autoradiography. FVIII HCs and LCs are indicated. The percentages of radiolabeled intracellular FVIII and secreted FVIII are shown relative to intracellular FVIII in lane 1. (iii) Secreted FVIII is functional by the activated partial thromboplastin time (aPTT) assay. (B) Inhibition of Glc metabolism and not oxidative phosphorylation causes FVIII aggregation. H9 cells treated with SAHA for 19 hours were subsequently treated with a mixture of 1 μM oligomycin A (Oligo) and 1 μM rotenone (Rot) which are complex II– and complex I–specific inhibitors of oxidative phosphorylation or 50 mM 2DG for indicated times (0-60 minutes). Cell lysates were filtered through CA membranes and probed with FVIII antibody. Blue bars represent technical duplicates. (C) FVIII aggregation is due to hydrophobic interactions. H9 cells treated with SAHA for 22 hours were treated with 20 mM 2DG and 10 mM NaN_3 for 2 hours. Treatment with tunicamycin (Tm), an ER stress inducer, started at 18 hours after SAHA. The percentage of FVIII retention on CA membranes was normalized to FVIII on NC membranes from technical duplicates. The longer exposure shows ~3% of the FVIII aggregates are resistant to 1% SDS.

the FVIII activity in the medium by ~50% (Figure 2Aii lane 9), indicating that approximately one-half of the FVIII activity was previously synthesized and was likely derived from FVIII aggregates. These findings support the conclusion that FVIII intracellular aggregates were dissolved and refolded for secretion of active FVIII.

Glucose metabolism promotes FVIII solubility

We then tested whether glycolysis and/or oxidative phosphorylation are required to prevent FVIII aggregation using specific inhibitors. Inhibition of Glc metabolism by 2DG immediately induced FVIII aggregation, where inhibition of oxidative phosphorylation by either oligomycin A (Oligo), a complex 5 inhibitor, or a combination of Oligo with rotenone (Rot), a complex 1 inhibitor, had no effect (Figure 2B; supplemental Figure 4D), indicating that Glc metabolism is required to solubilize FVIII. The role of Glc metabolism in reducing FVIII aggregates is under investigation. In addition, treatment with reducing agents dithiothreitol (DTT) or β-mercaptoethanol (β-ME) did not disrupt the aggregates, suggesting that they do not result from inappropriate disulfide bond crosslinking (supplemental Figure 4E). However, the FVIII aggregates in cell lysates were solubilized

with 1% SDS prior to CA membrane filtration (Figure 2C), although long exposure demonstrated that ~3% of the FVIII aggregates were resistant to 1% SDS, suggesting that FVIII aggregation is due to hydrophobic interactions.

A β-sheet within the FVIII A1 domain is necessary and sufficient for FVIII aggregation

We previously demonstrated that FV, which shares amino acid homology with FVIII, is very efficiently secreted from transfected mammalian cells compared with FVIII and does not significantly aggregate.[27] To identify the cause for inefficient FVIII secretion and aggregation, we studied FVIII/FV domain swap chimeras demonstrating that a 110-aa region (aa226-336) in the FVIII A1 domain is responsible for the inefficient secretion.[28] Furthermore, we identified hydrophobic motif aa291-310 in FVIII, which was absent in FV, for which mutations both enhanced (F309S mutation) or reduced (7LF>A mutation) secretion.[13,28] Importantly, the single mutation F309S, S being the homologous residue in FV (Figure 3A), completely conferred the efficient secretion of FV onto FVIII,[13] suggesting that aa291-310 predispose to FVIII aggregation. Hence, we analyzed mutants that increase (F309S and L303E/F309S [ES]), have a modest effect (L300V/L303E/F309S [VES] and L294T/L303E/F309S [TES]), or decrease (7LF>A [7 mutations of L and F to A, underlined in Figure 3A] and F306W) FVIII secretion by CA membrane retention. Mutations that increased FVIII secretion (F309S and ES) reduced retention and conversely, those that reduced secretion (7LF>A and F306W) increased retention when expressed in COS-1 (Figure 3B-C), CHO-K1 (not shown), or HepG2 (supplemental Figure 5) cells, indicating that this region is necessary for FVIII aggregation and is independent of the host cell type.

To test whether residues in the FVIII A1 domain are sufficient for aggregation, we introduced 79 residues (aa253-331) (supplemental Figure 6A) in frame into the enhanced green fluorescent protein (eGFP) fused to the human proinsulin C-peptide (Cpep) containing a cMyc tag (herein, CMy) (Figure 3D). Antibody to Cpep conveniently recognizes all of these chimeras. These 79 aa were chosen because they comprise the copper ion ligands at H267, C310, and H315 that might be important for maintaining FVIII structural integrity (supplemental Figure 6A). These chimeras have no glycosylation sites or disulfide bonds, therefore providing the ability to disentangle FVIII aggregation from posttranslational modifications. Fluorescence microscopy demonstrated significant green fluorescence in wild-type FVIII (wtFVIII)-eGFP-CMy expressing cells indicating that insertion of these 79 aa did not disrupt eGFP synthesis and folding (Figure 3E). Western blotting of cell lysates and media demonstrated that, in contrast to eGFP-CMy, insertion of the FVIII 79 aa into eGFP-CMy severely inhibited secretion that was further reduced by the multiple 7LF>A mutations (Figure 3F). Interestingly, secretion of the F309S and ES mutations in FVIII-eGFP-CMy was increased compared with wtFVIII-eGFP-CMy in 293T (Figure 3F) and HepG2 (supplemental Figure 7A-B) cells, indicating that these 79 aa are necessary and sufficient to seed aggregation. Notably, expression of FVIII-eGFP-CMy wt and all mutants caused ER stress–monitored BiP induction in transfected cells (Figure 3F). Thus, we propose that these 79 aa, termed Aggron, seed FVIII amyloid formation.

Application of the Tango algorithm, which predicts cross β-sheet propensity,[29] to the 79 aa identified 2 regions that can form β-sheets (supplemental Figure 8). Although C310S substitution did not alter the Tango plot, F309S or C310E substitutions or the respective 79 aa from FV eliminated the second β-sheet at F309. In contrast, F306W substitution, which further reduces secretion, enhanced the peak at F309. The F309S and C310E mutations in FVIII-eGFP-CMy were expressed in 293T (Figure 3G-H) and HepG2 (supplemental Figure 9) cells for analysis by CA membrane filtration and sucrose gradient sedimentation. In contrast to eGFP-CMy without the FVIII sequence, which migrated in light fractions 2-4, the majority of wtFVIII-eGFP-CMy migrated in heavy fractions 5-10 (Figure 3H-I). Compared to wtFVIII-eGFP-CMy, ~10-fold more F309SFVIII-eGFP-CMy and C310EFVIII-eGFP-CMy migrated in fraction 3 and ~20% less migrated in heavy fractions 9-10, indicating improved solubility of these mutants. These results support the validity of the Tango analysis and show that both F309 and C310 significantly contribute to FVIII aggregation. The C310 mutants C310S and C310E were both retained on CA membranes (supplemental Figure 10), suggesting that FVIII-eGFP-CMy aggregation is not mediated by an intermolecular disulfide linkage.

The aggregation properties of the 79 aa were further analyzed by removing eGFP to study wt and F309S FVIII-CMy in context of a smaller peptide (Figure 4A). For controls, CMy was expressed alone or with insertions of eGFP (eGFP-CMy) or the homologous residues from FV (FV-CMy). These polypeptides were detected in transfected 293T cells by western blotting (supplemental Figure 6B). Cpep enzyme-linked immunosorbent assay (ELISA) revealed that wtFVIII-CMy was poorly secreted, where FV-CMy and F309S FVIII-CMy secretion was approximately fivefold to ~10-fold greater (Figure 4B). However, secretion of the unrelated controls CMy or GFP-CMy was significantly further increased over FV-CMy and F309S FVIII-CMy. Inversely correlating with secretion, wtFVIII-CMy was retained upon CA membrane filtration, whereas F309S FVIII-CMy retention was reduced to 60% (Figure 4C). CA membrane retention of eGFP-CMy and FV-CMy was not detectable (Figure 4C). Sucrose gradient sedimentation also demonstrated reduced aggregation for F309S FVIII-CMy (Figure 4D-E). We next tested whether the wtFVIII-CMy aggregates have properties similar to full-length wtFVIII aggregates. Analysis of sucrose gradient fractions 3 and 10 from 293T cells that express wtFVIII-CMy demonstrated that wtFVIII-CMy was sensitive to 1% SDS but resistant to DTT and β-ME (Figure 4F). Together, these findings confirm that the 79 aa seed aggregation of structures that appear biochemically similar to wtFVIII.

Because 2DG treatment of H9 cells caused wtFVIII aggregation, we tested whether 2DG causes the short wtFVIII-CMy chimera to aggregate. Indeed, 2DG and NaN_3 treatment increased wtFVIII-CMy aggregation monitored by CA membrane filtration, with only a slight reduction in expression (Figure 4G; supplemental Figure 6B). These metabolic inhibitors did not significantly cause aggregation of CMy, FV-CMy, or eGFP-CMy. In addition, recovery of 2DG-treated cells in Glc-containing media decreased wtFVIII-CMy aggregation ~50% (Figure 4G), consistent with observations of wtFVIII in

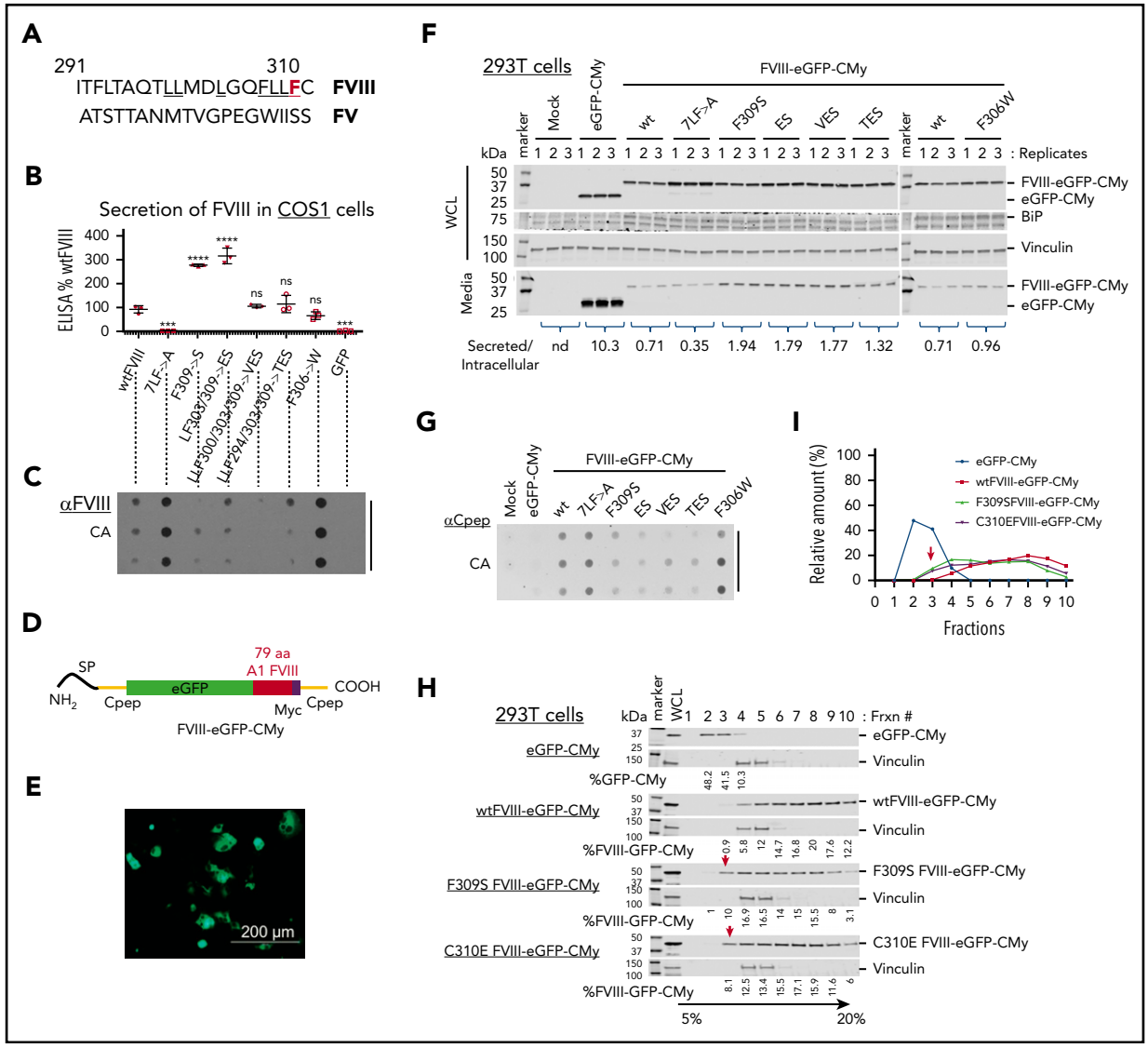

Figure 3. A short amino acid motif in the A1 domain seeds FVIII aggregation. (A) Homology between human FVIII and FV is shown between aa 291 and 310, with FVIII-F309 highlighted in red. (B-C) Mutations in the FVIII A1 domain exhibit different secretion efficiencies. COS-1 cells were transfected with expression vectors encoding single or multiple FVIII A1 mutations. 7LF>A has 7 Phe or Leu mutations to Ala underlined in panel A. At 48 hours after transfection, intracellular and secreted FVIII antigen were measured by ELISA. (B) Secreted FVIII relative to wtFVIII is shown as mean plus or minus standard deviation (SD) from biological triplicates. The results represented are from 1 experiment where similar results were reproducible in HepG2 cells (supplemental Figure 5). Statistical differences compared with wtFVIII were quantified by 1-way ANOVA using GraphPad Prism software: ****$P < .0001$; ***$P < .001$. Black bars represent biological replicates. (C) Lysates from transfected cells (the same as in panel B) were filtered through CA membranes to measure FVIII retention. (D-G) Seventy-nine amino acid seed FVIII aggregation. (D) Schematic structure is shown for FVIII-eGFP-CMy chimeras. The FVIII 79 aa were inserted in frame downstream of eGFP and upstream of the human proinsulin C peptide (Cpep) with a Myc tag (eGFP-CMy). The Myc tag is highlighted in purple and human Cpep is in yellow. (E) wtFVIII-eGFP-CMy–transfected cells were analyzed by fluorescence microscopy (fluorescence from enhanced green fluorescence protein; scale bar, 200 μm). (F-G) Mutations within 79 aa exhibit different FVIII-eGFP-CMy secretion and aggregation. (F) Intracellular and secreted FVIII-eGFP-CMy from 293T cells expressing wtFVIII-eGFP-CMy or different mutants (wt, 7LF>A, F309S, ES, VES, TES, and F306W) was analyzed by western blotting using Cpep antibody. The same membranes were probed with BiP and vinculin antibodies. Relative protein secretion vs intracellular protein is shown from 1 experiment with biological triplicates. (G) The protein samples in panel F were analyzed by filtration on CA membranes and probing with Cpep antibody. Similar results were observed in HepG2-transfected cells (supplemental Figure 7). (H-I) wtFVIII-eGFP-CMy forms HMW complexes. Cell lysates from 293T cells expressing wtFVIII-eGFP-CMy or mutant FVIII-eGFP-CMy were subjected to 5% to 20% sucrose gradient sedimentation. Proteins from fractions 1 to 10 were analyzed by western blot using Cpep antibody. The membrane was probed with vinculin antibody for loading control. The proportion of protein in each fraction is indicated as a percentage of total and plotted in panel I. Red arrows indicate migration of soluble forms of F309S FVIII-eGFP-CMy and Cys310Glu mutation of FVIII-eGFP-CMy (C310E FVIII-eGFP-CMy). A similar finding was observed in HepG2-transfected cells (supplemental Figure 9). Frxn, fraction; nd, not determined; SP, the proinsulin signal peptide; WCL, whole-cell lysate.

H9 and 10A1 cells. This suggests that FVIII aggregation was not simply a consequence of altered glycosylation in response to 2DG because wtFVIII-CMy contains no *N*-linked glycans.

Finally, the potential of wtFVIII-CMy to form intermolecular heterodimers/oligomers with FVIII was investigated. wtFVIII-CMy and full-length FVIII or B-domain–deleted (BDD) FVIII, which aggregates similarly to FVIII (not shown), were coexpressed in 293T cells (supplemental Figure 11) and their interaction was analyzed by coimmunoprecipitation (co-IP). Surprisingly, Cpep IP of the short chimera wtFVIII-CMy efficiently pulled-down both wtFVIII and BDD-FVIII (Figure 4H), suggesting

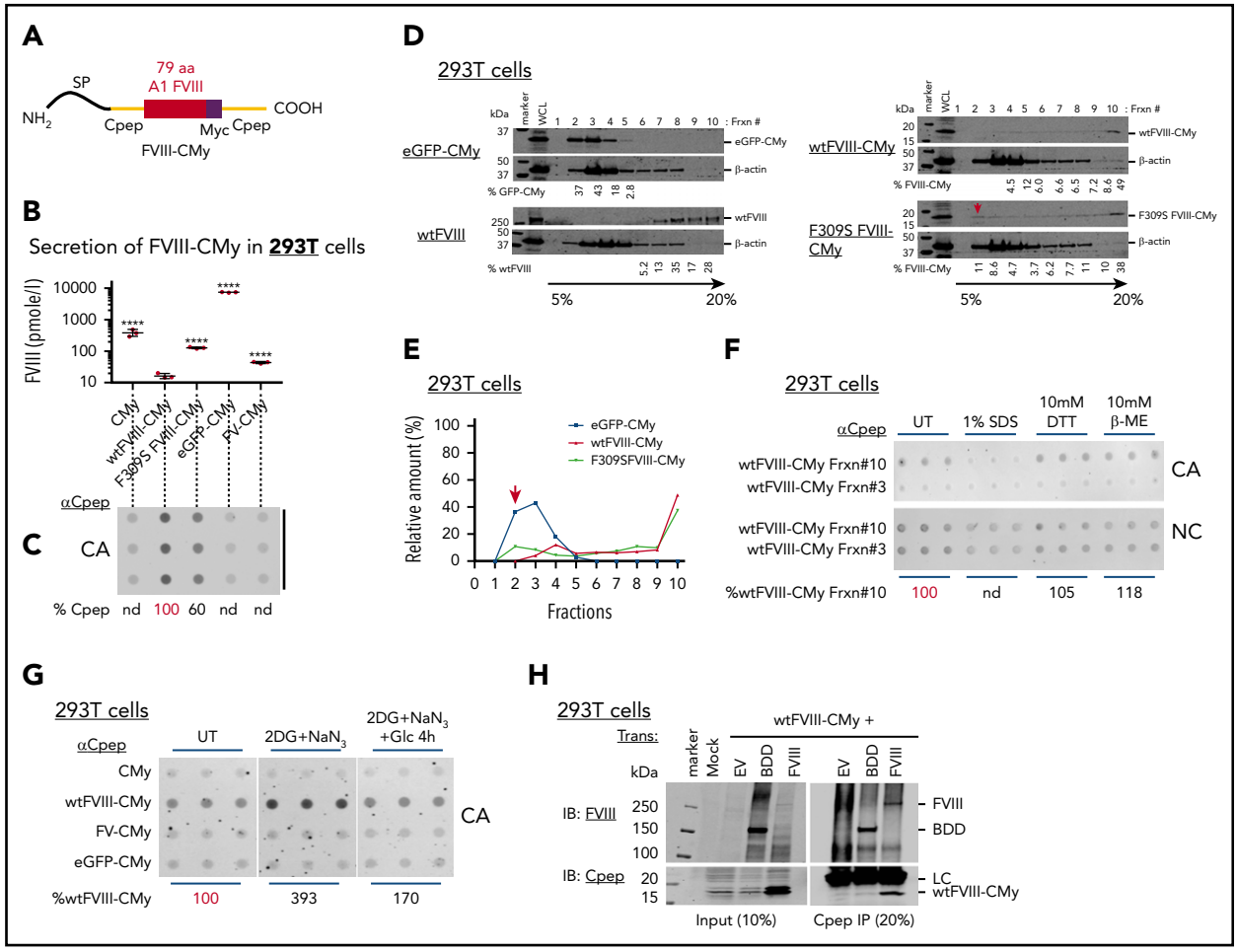

Figure 4. Seventy-nine amino acids from FVIII mediate Cpep-reversible aggregation upon restoration of Glc metabolism. (A) Schematic shows structure of the FVIII 79 aa inserted in frame upstream of the human proinsulin C peptide (Cpep) with a Myc tag to generate wtFVIII-CMy. Cys329 at the carboxy terminus of the 79 aa in the FVIII A1 domain was mutated to Gly to prevent aberrant disulfide bond formation (supplemental Figure 6A). (B-C) Seventy-nine amino acids from FVIII cause Cpep aggregation. 293T cells were transfected with indicated expression plasmids. (B) At 48 hours posttransfection, culture media was analyzed by Cpep ELISA and results presented secreted Cpep as mean plus or minus SD on $\log_{10}$ scale. Statistical analysis of secretion compared with wtFVIII-Cpep was performed by 1-way ANOVA using GraphPad Prism software. $^{****}P < .0001$. (C) At 48 hours posttransfection, cell lysates were analyzed for retention on CA membranes by probing with Cpep antibody. Data shown are from a representative experiment with biological triplicates. eGFP-CMy and FV-CMy, constructed as similar as the FVIII-CMy chimera, transfection was included as another control. (D) wtFVIII-Cpep forms in HMW complexes. Cell lysates from 293T expressing wtFVIII-CMy, F309S FVIII-CMy, and eGFP-CMy were analyzed by 5% to 20% sucrose gradient sedimentation as in Figure 3H. Protein samples from 1 to 10 fractions were analyzed by western blotting using Cpep antibody. Sucrose gradient sedimentation of cell lysate from wtFVIII-transfected cells was performed in parallel. (E) The proportion of protein in each fraction is indicated as a percentage of total. Red arrows in panels D and E indicate migration of soluble forms of F309S FVIII-CMy. (F) wtFVIII-CMy aggregation is mediated by hydrophobic interactions but not disulfide cross-links. Sucrose gradient fractions 3 and 10 were treated with/without 1% SDS or with reducing agents (10 mM DTT or 10 mM β-ME) before CA filtration and probing with Cpep antibody. Blue bars represent technical triplicates. The percentage of FVIII on CA membranes is shown as relative to untreated (UT). (G) Aggregation of wtFVIII-CMy is reversible and requires Glc. 293T cells expressing either CMy, wtFVIII-CMy, FV-CMy, or eGFP-CMy were untreated or treated with Glc-free Dulbecco's Modified Eagles Medium (DMEM) containing 20 mM 2DG and 10 mM NaN_3 for 2.5 hours. For repletion, the 2DG and NaN_3–containing medium was replaced with DMEM (25 mM glucose) and cells were cultured 4 hours. Finally, cell lysates were filtered through CA and NC membranes and probed with Cpep antibody. Blue bars = technical triplicates. The percentage of aggregated wtFVIII-CMy is relative to untreated. (H) wtFVIII-CMy specifically interacts with BDD and wtFVIII. Cell lysates from cells cotransfected with wtFVIII-CMy and wtFVIII or BDD-FVIII were immunoprecipitated with Cpep antibody. Both input and Cpep-immunoprecipitated protein were analyzed by western blot probed by FVIII antibody (Baxter) and Cpep antibody. EV, empty vector; Frxn, fraction; SP, proinsulin signal peptide.

that these 79 aa interact in *trans* to alter the wtFVIII folding pathway.

BiP and CANX/CRT prevent FVIII aggregation in the ER

Mass spectrometry of FVIII immunoprecipitated from control CHO cells and H9 cells treated with NaB identified many ER chaperones and enzymes that selectively interact with wtFVIII (supplemental Figure 12A-B). FVIII interactions with BiP, CANX, UGGT1, SEL1L, and PDIA6 were validated by FVIII IP and western blotting (supplemental Figure 12C). PDIA6 also colocalized with FVIII by immunogold TEM (Figure 1C).

The 2 most significant FVIII interactors were BiP/GRP78/HSPA5 and its cochaperones (ERdj5, ERdj3, and GRP170) and CANX/CRT with its associated factors UGGT1 and ERP57/PDIA3, raising the question of whether these chaperones influence FVIII aggregation. Complete inhibition of the CANX/CRT cycle with castanospermine (CST), an inhibitor of α-glucosidase (GS1 and GS2) activity, increased FVIII aggregation without altering FVIII expression (supplemental Figure 13A-C), suggesting that CANX/CRT prevents wtFVIII aggregation, possibly by binding soluble monoglucosylated *N*-linked glycans on FVIII. However, CST treatment of cells expressing the wtFVIII-CMy short chimera did not significantly increase wtFVIII-CMy aggregation

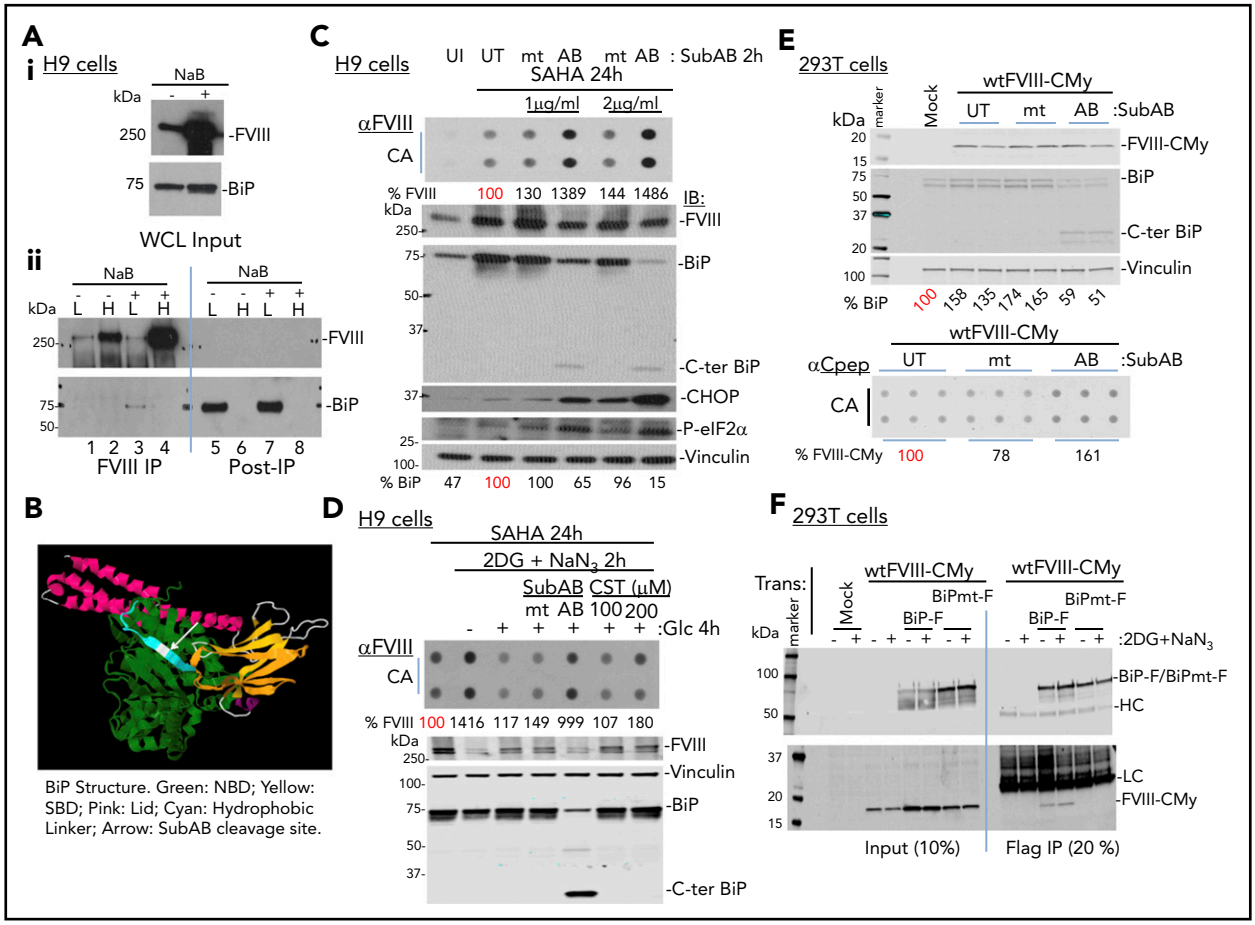

Figure 5. Upon Glc replenishment, BiP ATPase activity is required to solubilize wtFVIII-CMy. (A) BiP binds LMW-FVIII. Lysates from H9 cells treated with or without NaB were subjected to sucrose gradient sedimentation, and FVIII from fractions 5 (light fraction [L]) and 10 (heavy fraction [H]) was immunoprecipitated. After elution, coimmunoprecipitated BiP was analyzed by western blotting with FVIII and BiP antibodies. (i) Western blots for FVIII and BiP are shown for cell lysates. (ii) Western blots are shown for FVIII IP and post-IP supernatants. (B) The figure shows the crystal structure of BiP in the ATP-bound conformation. The white arrow indicates the cleavage site for SubAB protease that connects the nucleotide-binding domain (NBD; green) with the substrate-binding domain (SBD; yellow). The C-terminal lid is indicated in pink. The model is based on PDB-6ASY.[56] (C) BiP cleavage induces wtFVIII aggregation. H9 cells were treated with 5 μM SAHA for 24 hours and BiP cleavage was initiated by treating cells with 1 or 2 μg/mL SubAB (AB) or mutant $SubA_{272}B$ (mt) for the last 2 hours of SAHA treatment. Top, CA membrane filtration of cell lysates shows relative levels of FVIII aggregation compared with cells not treated with SubAB (UT). Bottom, Western blot is shown for cell lysates using indicated antibodies. The abundance of intact BiP (~75 kDa) was quantified relative to vinculin (loading control) and is represented as a percentage of untreated. (D) BiP is required for disassociation of FVIII aggregates. H9 cells treated with SAHA for 18 hours and then with 2DG and NaN_3 for 2 hours in the absence of Glc. Then, Glc was repleted in the presence of either 2 μg/mL SubAB (AB) or $SubA_{272}B$ (mt) or CST (100 and 200 μM) for 4 hours. Cell lysates were filtered through a CA membrane and analyzed by blotting. The percentage of FVIII aggregation was quantified from the FVIII signals on CA relative to western blotting compared with untreated control. C-ter BiP is SubAB cleaved C-terminal BiP. (E) BiP inactivation induces wtFVIII-CMy aggregation. 293T cells expressing wtFVIII-CMy were treated with or without SubAB or mtSubAB (2 μg/mL) for 2.5 hours and then harvested for western blotting and CA membrane filtration. The relative wtFVIII-CMy western blot intensities were normalized to vinculin. CA intensities were normalized to FVIII western blot intensities. Black bars = biological duplicates; blue bars = technical triplicates. These data are a representative experiment with biological duplicates. (F) wtFVIII-CMy interacts with BiP. Cell lysates from 293T cells expressing wtFVIII-CMy and BiP-Flag (BiP-F) or BiP-Flag (V461F) (BiPmt-F), a peptide-binding defective mutant, were used for Flag IP. After IP and blotting, BiP was detected with Flag antibody (top) and FVIII-CMy with Cpep antibody (bottom) to compare untreated cells and cells treated with 2DG and NaN_3 for 2.5 hours. LC and HC represent immunoglobulin light and heavy chains of Flag antibody. UI, uninduced.

(supplemental Figure 13D-E), confirming that aggregation of the 79 aa is not due to altered glycosylation because this chimera has no *N*-glycans.

To study the role of BiP in FVIII aggregation, we analyzed whether BiP binds to low-molecular-weight (LMW) and/or HMW FVIII species. Cell lysates from NaB-treated H9 cells were analyzed before (Figure 5Ai) and after sucrose gradient sedimentation (Figure 5Aii) by FVIII IP and western blotting. Although similar amounts of FVIII migrated in LMW fraction 5 (L) from both untreated and NaB-treated H9 cells (Figure 5Aii lanes 1, 3), there was a vast amount of FVIII in the HMW fraction 10 (H) (Figure 5Aii lane 2), with even more upon NaB induction (Figure 5Aii lane 4). FVIII IP and western blotting demonstrated detectable BiP interaction only with the LMW fraction 5 of FVIII from NaB-treated, and not in untreated, H9 cells (Figure 5Aii lanes1, 3). BiP was not detected in the HMW fraction (Figure 5ii lanes 2, 4), nor did we detect BiP in the postimmunoprecipitation (post-IP) HMW sucrose fraction supernatant (Figure 5Aii lanes 6, 8). Significantly, the majority of BiP was detected in the FVIII post-IP supernatant in the LMW fraction (Figure 5Aii lanes 5, 7). Collectively, these data suggest that BiP preferentially associates with LMW FVIII.

To further analyze how BiP impacts FVIII aggregation, we used the Shiga-toxic *Escherichia coli* virulence factor $SubA_{272}B_{mt}$

(SubAB), which specifically and acutely cleaves at a single site in the hydrophobic linker that connects the BiP amino-terminal ATPase domain with the substrate-binding domain (Figure 5B).[30,31] As control, cells were treated with a protease-mutant SubAB. Treatment of cells with 1 or 2 μg/mL of the active protease acutely cleaved ~35% and ~85% of BiP, respectively, and increased FVIII aggregation detected by retention on CA membranes (Figure 5C), suggesting that intact BiP, but not cleaved BiP, prevents FVIII aggregation. BiP cleavage was associated with UPR activation by induction of phosphorylated eukaryotic initiation factor 2 α (P-eIF2α) and CHOP (Figure 5C), consistent with previous findings.[32]

Although these results indicate that BiP and CANX/CRT prevent FVIII aggregation, they do not address their role in disaggregation. Hence, we treated H9 cells with NaB for 18 hours with the last 2 hours in the presence of 2DG and NaN_3 to induce maximal FVIII aggregation. Then, fresh media with Glc were added for 4 hours in the presence or absence of SubAB protease or CST. Although 2DG and NaN_3 reduced FVIII expression, BiP cleavage prevented the Glc-dependent dissociation of FVIII aggregates (Figure 5D). In contrast, inactivation of the CANX/CRT cycle by CST did not significantly prevent disaggregation. Collectively, we conclude that BiP, and not CANX/CRT, is required to disaggregate polymerized FVIII.

To evaluate the role of BiP in preventing FVIII aggregation, BDD-FVIII, for which aggregation is induced by BiP inactivation similarly to wtFVIII (supplemental Figure 11), was coexpressed with Flag-tagged BiP (BiP-F), mutant V461FBiP-Flag (BiPmt-F), which is peptide-binding defective,[33] or Myc-tagged BiP (BiP-M).[33] Forced expression of BiP-F or BiP-M did not alter BDD-FVIII expression, although they significantly reduced BDD-FVIII aggregation measured by retention on CA membranes (supplemental Figure 14). In addition, the V461F mutant BiP was partially defective in preventing BDD-FVIII aggregation. Thus, we conclude that BiP requires its peptide-binding site to efficiently promote FVIII solubility in the ER.

We next tested whether BiP cleavage by SubAB impacts aggregation of the wtFVIII-CMy chimera. 293T cells expressing wtFVIII-CMy were treated with mt or wtSubAB. After 2.5 hours, ~40% to 50% of BiP was cleaved without affecting wtFVIII-CMy expression (Figure 5E top). Compared with mtSubAB treatment control, wtFVIII-CMy aggregation increased ~60% upon BiP cleavage (Figure 5E bottom). Although SubAB inhibits secretion of immunoglobulin,[34] secretion of eGFP-CMy was not reduced (supplemental Figure 15A-B), indicating that the secretory pathway remained intact. Collectively, these findings show that intact BiP prevents aggregation of wtFVIII-CMy through interaction with the BiP peptide-binding site.

BiP interacts with wtFVIII-CMy to prevent aggregation

We finally tested whether BiP binds to the 79 aa by coexpression of wtFVIII-CMy with BiP-F or the peptide-binding defective BiPmt-F.[33] Indeed, Flag IP of BiP coimmunoprecipitated wtFVIII-CMy (Figure 5F), suggesting a direct interaction between BiP and the 79 aa of FVIII. In contrast, Flag IP of mutant BiPmt-F did not co-IP. However, treatment with 2DG and NaN_3 did not significantly increase the BiP-wtFVIII-CMy interaction, consistent with the notion that SubAB toxin cleavage of BiP induces wtFVIII-CMy aggregation, as we could not detect BiP binding to HMW FVIII aggregates (Figure 5A). However, mutations that reduce FVIII-CMy aggregation did not detectably alter BiP interaction measured by co-IP (not shown). It is likely that BiP binds multiple sequences so mutations that reduce aggregation do not alter BiP interaction, as previously suggested.[35,36] These findings support the conclusion that BiP binds 79 aa in wtFVIII-CMy to prevent aggregation.

Discussion

FVIII forms reversible amyloid-like aggregates in the ER

FVIII is poorly secreted due to retention in the ER. Here, we provide significant insight into the mechanism for FVIII retention in the ER. We demonstrated that FVIII forms amyloid-like fibrils in the ER when expression is constitutively high and, to a greater extent, upon increased synthesis. In addition, inhibition of Glc metabolism, but not oxidative phosphorylation, causes FVIII aggregation and reduces secretion. The following characterize the demonstrated amyloid fibril properties of these aggregates: (1) sucrose gradient fractionation of cell lysates, FVIII pulse-chase labeling and IP, negative-stain TEM, and cryo-EM, which identified ~5-nm fibrils and fibril networks only in the very HMW gradient fractions; (2) FVIII colocalization with Thio-S in the ER; (3) FVIII retention on CA membranes; (4) immunogold TEM showing FVIII clustering with the ER-localized PDIA6; and (5) sensitivity to 1% SDS, although a small fraction (~3%) was resistant, possibly analogous to prefibrillar conversion to fibrillar amyloid structures that undergo transition from SDS-sensitive to SDS-resistant forms.[37,38] Other than immunoglobulin LC and HCs,[39] this represents a unique example of amyloid-like aggregates formed in the ER. Remarkably, unlike other amyloids, FVIII aggregates were reversible upon Glc supplementation and were recovered as functional FVIII secreted into the medium. To our knowledge, this is the first example of reversible amyloidogenesis leading to proper folding of a protein in metazoans.

BiP and CANX/CRT prevent FVIII aggregation

Mass spectrometry demonstrated FVIII interaction with BiP and CANX/CRT. Here, we show that CANX/CRT interaction reduces wtFVIII aggregation, similar to other glycoproteins.[40,41] BiP preferentially binds to LMW FVIII and not HMW FVIII aggregates. BiP inactivation increased FVIII aggregation, and forced BiP expression reduced FVIII aggregation. Thus, BiP is required to prevent FVIII aggregation and/or to mediate disaggregation. It was shown that increased BiP expression inhibits wtFVIII secretion.[14] However, contrary to what we expected, increased BiP expression prevented wtFVIII aggregation and retained soluble LMW FVIII in the ER. From these findings, we propose a model for BiP function in preventing FVIII amyloid formation (Figure 6A).

Identification of the β-aggregate–seeding motif in the FVIII A1 domain

To further characterize FVIII aggregation, we identified 79 aa in the A1 domain that seed β-aggregation. Expression of a chimeric polypeptide (wtFVIII-eGFP-CMy or wtFVIII-CMy) recapitulated the major aspects of wtFVIII aggregation including: (1) wtFVIII-CMy aggregated in response to glycolysis inhibition and (2) wtFVIII-CMy aggregated in response to BiP cleavage and inactivation by SubAB cytotoxin. In addition, we show that the

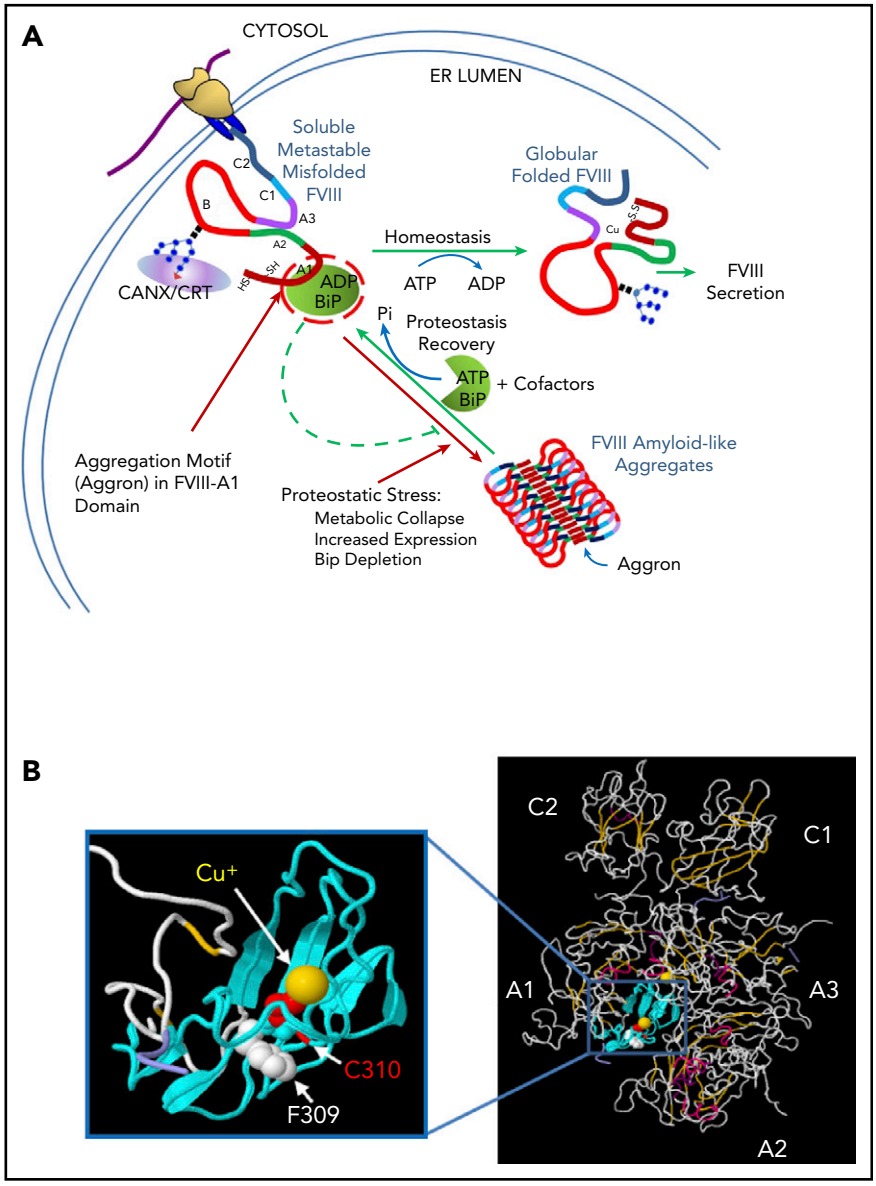

Figure 6. Models depict mechanism for reversible FVIII amyloid formation and for impact of F309S mutation on FVIII structure. (A) BiP regulates reversible FVIII amyloidogenesis in the ER lumen. Once nascent FVIII (A1-A2-B-A3-C1-C2) translocates into the ER lumen, it undergoes *N*-linked core oligosaccharide addition and disulfide bond formation. Glycosylated FVIII subsequently interacts with the lectin chaperones CANX/CRT and the peptide-binding protein BiP. BiP binds FVIII within a short sequence aggregating motif (Aggron) in the A1 domain to facilitate folding by preventing aggregation and stabilizing soluble misfolded, but folding-competent, FVIII. Upon release from CANX/CRT correctly folded FVIII (soluble) traffics to the Golgi compartment. Glc supplementation produces ATP by glycolysis to activate the BiP ATPase cycle (client binding and release[57]) that stimulates FVIII disaggregation and BiP release for FVIII folding and secretion as a functional clotting factor. Under proteostatic stress, such as increased FVIII expression, metabolic collapse or BiP depletion, FVIII misfolds and forms amyloid-like fibrils due to antiparallel β-sheet polymerization initiated by the Aggron (aa 253-331) in the FVIII A1 domain. The Aggron- and BiP-binding site in the A1 domain overlap is indicated by the red circle. Red lines depict pathways of aggregation; green lines depict productive folding. (B) F309S reduces amyloidogenesis as well as Cu^{+} interaction with C310. The 3-dimensional FVIII structure (A1-A2-A3-C1-C2 domains)[16,17] is shown where the 79 aa (residues 253-331) in the A1 domain are colored cyan also showing the phenylalanine (F, white) residue 309 and cysteine (C, red) residue 310 in the A1 domain. The Cu^{+} ions in the A1 and A3 domains are colored yellow. This predicted FVIII crystal structure was processed using Jsmol software. We propose that the hydrophobic patch aa 253-331 enforces tight Cu^{+} interaction with C310. Mutation of F309S (S being the homologus residue in FV that does not ligand copper ion) reduces FVIII aggregation and increases secretion. From the FVIII crystal structure, mutant F309S replaces a large hydrophobic side chain with a smaller polar one. Therefore, F309 FVIII would bind copper ion more avidly than S309 FVIII, although at the same time increasing aggregation propensity. ADP, adenosine 5′-diphosphate; HS/SH, thiols; Pi, phosphate.

79-aa motif interacts in *trans* with wtFVIII and BDD-FVIII as well as with the peptide-binding site on BiP. We propose that BiP binding to the FVIII aggregate-seeding region, Aggron, prevents aggregation, consistent with previous reports of other proteins.[35,42,43] As BiP prevents FVIII aggregation, it is interesting to note that 3 BiP cochaperones, ERdj3, ERdj5, and GRP170, the latter 2 of which interact with aggregation-prone sequences,[35] were also identified as significant interactors with wtFVIII. Although previous studies linked cochaperone interactions with ER-associated degradation, FVIII is not significantly degraded by ER-associated degradation, but rather is secreted. Present studies are testing the significance of these cochaperone interactions. Importantly, without the complication from glycosylation sites and disulfide bonds, wtFVIII-CMy did not aggregate upon inhibition of the CANX/CRT cycle, implicating the glycans as important for wtFVIII solubility. Finally, these observations on FVIII aggregation were cell-type independent as they were observed in CHO, 293T, COS-1, and HepG2 cells.

Can FVIII aggregation impact human HA gene therapy?

At least 3 HA gene therapy clinical trials are in progress delivering BDD-FVIII in adeno-associated viral vectors (AAVs) to hepatocytes (https://clinicaltrials.gov/ct2/results?term =hemophilia+a+gene+therapy). One report demonstrated significant success in 9 men with severe HA at 1 year after virus delivery to obtain 100% FVIII levels in the blood.[44] However, a more recent update indicated the FVIII levels in the high-dose cohort (6e13 vector genomes per kilogram) decreased ~50% after year 2,[45] which is unusual compared with the stable expression observed in other hepatocyte-directed AAV gene-therapy trials.[46,47] All of the properties of wtFVIII misfolding and aggregation also exist for BDD-FVIII that is presently used in HA gene-therapy clinical studies.[9] It should be considered that the decline in FVIII expression may reflect toxicity of aggregated BDD-FVIII in hepatocytes. In addition, endogenous FVIII is not likely expressed in hepatocytes, but rather in Kupffer cells and sinusoidal

endothelial cells,[48-50] which may harbor machinery to efficiently fold FVIII. We also observed aggregation of BDD-FVIII in hepatocytes of mice that received BDD-FVIII DNA expression vectors (data not shown). In addition, ER stress was induced in livers upon DNA delivery of BDD-FVIII to mice in vivo,[9] consistent with ER stress detected upon AAV delivery of BDD-FVIII.[51,52] Recently, it was shown that ER protein misfolding in hepatocytes with subsequent inflammation caused by a high-fat diet in mice can initiate nonalcoholic fatty liver disease with progression to nonalcoholic steatohepatitis and hepatocellular carcinoma.[53] Thus, it will be important to monitor liver function in the HA gene-therapy studies.

Importantly, why does FVIII harbor an Aggron in the A1 domain? Intriguingly, the Aggron includes Cys310, which ligands Cu^{+} in functional wtFVIII.[15] Of all amino acid variants that reduce FVIII aggregation and improve secretion, F309S was the most effective. Previously, it was demonstrated that F309S FVIII exhibits clotting factor–specific activity, thermal denaturation, and thrombin activation indistinguishable from wtFVIII.[13] However, F309S FVIII was 10-fold more sensitive to EDTA inactivation, which presumably extracts Cu^{+}. The F309S mutation substitutes a large, hydrophobic side chain with a smaller, more polar, one, and may increase flexibility to relax the C310 interaction with Cu^{+} (Figure 6B). Although the potential of neoantigenicity of F309S mutation has not been addressed, F309 is buried within the FVIII 3-dimensional structure[16,17] and may not be accessible to the immune response. Because F309S FVIII and F309S BDD-FVIII function identically to wtFVIII and BDD-FVIII, respectively, display lesser aggregation and lesser UPR activation, and are secreted more efficiently, they may be considered an alternative choice to wtFVIII or BDD-FVIII for HA gene therapy. Finally, along these lines, because increased plasma FVIII levels associate with venous thrombosis,[54,55] our findings should encourage evaluating whether F309S FVIII mutation associates with thrombosis in humans.

Acknowledgments

The authors thank David Ron for kindly providing BiP expression vectors, and Peter Arvan and Ming Liu for providing the pTargetT-hProCpepMyc and pTarget-hProCpepeGFP vector. Baxter Corp (Deerfield, IL) kindly provided FVIII antibody-conjugated sepharose beads. The authors gratefully thank Michael Cunningham for performing the TEM of FVIII fibrils (Figure 1D), Lisa Giles for analyzing immunofluorescence and establishing the CA filter-binding assay (Figure 1B and supplemental Figure 4), and Jyoti Malhotra for performing pulse-chase radiolabeling and IP (Figure 2Aii). Immunogold labeling and TEM was performed at the University of California San Diego (UCSD) Cellular and Molecular Medicine Electron Microscopy Facility. The authors thank the University of Michigan Transmission Electron Microscopy Laboratory for analysis of negative-stained purified FVIII fibrils. The authors thank Peter Arvan for critical review of this manuscript.

This work was supported by the following National Institutes of Health grants: R01HL052173 (National Heart, Lung, and Blood Institute; R.J.K.); R37DK042394, R01DK113171 (R.J.K.), R01DK103185 (R.J.K.), and R24DK110973 (R.J.K.) (all 4 from the National Institute of Diabetes and Digestive and Kidney Diseases); R01CA198103 (National Cancer Institute; R.J.K.); R01AG062190 (National Institute on Aging; R.J.K.); and P30 CA030199 (National Cancer Institute SBP Cancer Center). The cryo-EM studies were supported by National Institutes of Health grants R01GM119948 (National Institute of General Medical Sciences; D.H., N.V.) and S10-OD012372 (Office of the Director; D.H.).

R.J.K. is a member of the UCSD Diabetes Research Center (P30 DK063491 [National Institute of Diabetes and Digestive and Kidney Diseases]) and is an adjunct professor in the Department of Pharmacology, UCSD.

Authorship

Contribution: J.P. performed all studies on FVIII-CMy and FVIII-eGFP-CMy, designed the experiment, and wrote the manuscript; Z.C. provided expert consultation and assisted in manuscript preparation; J.Y. performed sucrose gradient analyses and BiP interaction and prepared the manuscript; A.R.C. performed mass spectrometry analyses and bioinformatics; A.P. performed mass spectrometry analyses and experiments to validate the significance of FVIII-interacting proteins; J.Y., M. Swift, D.H., and N.V. performed the cryo-EM sample preparation and analysis; D.H. and N.V. provided financial support for the cryo-EM studies; J.L.-A. provided technical support; M. Siirin performed studies involving CA and NC membrane filtration and analyses of FVIII secretion and the intracellular ATP level; A.W.P. and J.C.P. provided essential reagents; and R.J.K. directed the studies, assured validity of findings, wrote the manuscript, and provided financial support for the studies.

Conflict-of-interest disclosure: The authors declare no competing financial interests.

ORCID profiles: J.P., 0000-0002-6810-1807; J.Y., 0000-0002-4970-408X; R.J.K., 0000-0003-4277-316X.

Correspondence: Randal J. Kaufman, Degenerative Diseases Program, SBP Medical Discovery Institute, 10901 N. Torrey Pines Rd, La Jolla, CA 92037; e-mail: rkaufman@sbpdiscovery.org.

Footnotes

Submitted 27 August 2019; accepted 13 February 2020; prepublished online on *Blood* First Edition 3 March 2020. DOI 10.1182/blood.2019002867.

*J.P. and A.P. contributed equally to these studies.

The mass spectrometry data reported in this article have been submitted to the ProteomeXchange (submission number PXD015029).

The online version of this article contains a data supplement.

There is a *Blood* Commentary on this article in this issue.

The publication costs of this article were defrayed in part by page charge payment. Therefore, and solely to indicate this fact, this article is hereby marked "advertisement" in accordance with 18 USC section 1734.

REFERENCES

1. Toole JJ, Knopf JL, Wozney JM, et al. Molecular cloning of a cDNA encoding human antihaemophilic factor. *Nature*. 1984; 312(5992):342-347.
2. Vehar GA, Keyt B, Eaton D, et al. Structure of human factor VIII. *Nature*. 1984;312(5992): 337-342.
3. Kaufman RJ. Genetic engineering of factor VIII. *Nature*. 1989;342(6246):207-208.
4. Walter P, Ron D. The unfolded protein response: from stress pathway to homeostatic regulation. *Science*. 2011;334(6059):1081-1086.
5. Mori K. The unfolded protein response: the dawn of a new field. *Proc Jpn Acad, Ser B, Phys Biol Sci*. 2015;91(9):469-480.
6. Wang M, Kaufman RJ. Protein misfolding in the endoplasmic reticulum as a conduit to human disease. *Nature*. 2016;529(7586): 326-335.
7. Dorner AJ, Bole DG, Kaufman RJ. The relationship of N-linked glycosylation and heavy chain-binding protein association with the secretion of glycoproteins. *J Cell Biol*. 1987; 105(6 Pt 1):2665-2674.

8. Dorner AJ, Wasley LC, Kaufman RJ. Increased synthesis of secreted proteins induces expression of glucose-regulated proteins in butyrate-treated Chinese hamster ovary cells. *J Biol Chem*. 1989;264(34):20602-20607.

9. Malhotra JD, Miao H, Zhang K, et al. Antioxidants reduce endoplasmic reticulum stress and improve protein secretion. *Proc Natl Acad Sci USA*. 2008;105(47):18525-18530.

10. Zaitsev VN, Zaitseva I, Papiz M, Lindley PF. An x-ray crystallographic study of the binding sites of the azide inhibitor and organic substrates to ceruloplasmin, a multi-copper oxidase in the plasma. *J Biol Inorg Chem*. 1999;4(5):579-587.

11. Jenny RJ, Pittman DD, Toole JJ, et al. Complete cDNA and derived amino acid sequence of human factor V. *Proc Natl Acad Sci USA*. 1987;84(14):4846-4850.

12. Dorner AJ, Wasley LC, Kaufman RJ. Protein dissociation from GRP78 and secretion are blocked by depletion of cellular ATP levels. *Proc Natl Acad Sci USA*. 1990;87(19):7429-7432.

13. Swaroop M, Moussalli M, Pipe SW, Kaufman RJ. Mutagenesis of a potential immunoglobulin-binding protein-binding site enhances secretion of coagulation factor VIII. *J Biol Chem*. 1997;272(39):24121-24124.

14. Dorner AJ, Wasley LC, Kaufman RJ. Overexpression of GRP78 mitigates stress induction of glucose regulated proteins and blocks secretion of selective proteins in Chinese hamster ovary cells. *EMBO J*. 1992;11(4):1563-1571.

15. Tagliavacca L, Moon N, Dunham WR, Kaufman RJ. Identification and functional requirement of Cu(I) and its ligands within coagulation factor VIII. *J Biol Chem*. 1997;272(43):27428-27434.

16. Ngo JC, Huang M, Roth DA, Furie BC, Furie B. Crystal structure of human factor VIII: implications for the formation of the factor IXa-factor VIIIa complex. *Structure*. 2008;16(4):597-606.

17. Shen BW, Spiegel PC, Chang CH, et al. The tertiary structure and domain organization of coagulation factor VIII. *Blood*. 2008;111(3):1240-1247.

18. Kaufman RJ, Wasley LC, Dorner AJ. Synthesis, processing, and secretion of recombinant human factor VIII expressed in mammalian cells. *J Biol Chem*. 1988;263(13):6352-6362.

19. Tagliavacca L, Wang Q, Kaufman RJ. ATP-dependent dissociation of non-disulfide-linked aggregates of coagulation factor VIII is a rate-limiting step for secretion. *Biochemistry*. 2000;39(8):1973-1981.

20. Wanker EE, Scherzinger E, Heiser V, Sittler A, Eickhoff H, Lehrach H. Membrane filter assay for detection of amyloid-like polyglutamine-containing protein aggregates. *Methods enzymol*. 1999;309:375-386.

21. Wolfe LS, Calabrese MF, Nath A, Blaho DV, Miranker AD, Xiong Y. Protein-induced photophysical changes to the amyloid indicator dye thioflavin T. *Proc Natl Acad Sci USA*. 2010;107(39):16863-16868.

22. Groenning M. Binding mode of Thioflavin T and other molecular probes in the context of amyloid fibrils-current status. *J Chem Biol*. 2010;3(1):1-18.

23. Bäuerlein FJB, Saha I, Mishra A, et al. In situ architecture and cellular interactions of PolyQ inclusions. *Cell*. 2017;171(1):179-187.e10.

24. Shirahama T, Cohen AS. Structure of amyloid fibrils after negative staining and high-resolution electron microscopy. *Nature*. 1965;206(985):737-738.

25. Nizynski B, Nieznanska H, Dec R, Boyko S, Dzwolak W, Nieznanski K. Amyloidogenic cross-seeding of Tau protein: transient emergence of structural variants of fibrils. *PLoS One*. 2018;13(7):e0201182.

26. Ivanova MI, Sievers SA, Guenther EL, et al. Aggregation-triggering segments of SOD1 fibril formation support a common pathway for familial and sporadic ALS. *Proc Natl Acad Sci USA*. 2014;111(1):197-201.

27. Pittman DD, Tomkinson KN, Kaufman RJ. Post-translational requirements for functional factor V and factor VIII secretion in mammalian cells. *J Biol Chem*. 1994;269(25):17329-17337.

28. Marquette KA, Pittman DD, Kaufman RJ. A 110-amino acid region within the A1-domain of coagulation factor VIII inhibits secretion from mammalian cells. *J Biol Chem*. 1995;270(17):10297-10303.

29. Fernandez-Escamilla AM, Rousseau F, Schymkowitz J, Serrano L. Prediction of sequence-dependent and mutational effects on the aggregation of peptides and proteins. *Nat Biotechnol*. 2004;22(10):1302-1306.

30. Paton AW, Beddoe T, Thorpe CM, et al. AB5 subtilase cytotoxin inactivates the endoplasmic reticulum chaperone BiP. *Nature*. 2006;443(7111):548-552.

31. Yang J, Zong Y, Su J, et al. Conformation transitions of the polypeptide-binding pocket support an active substrate release from Hsp70s. *Nat Commun*. 2017;8(1):1201.

32. Wolfson JJ, May KL, Thorpe CM, Jandhyala DM, Paton JC, Paton AW. Subtilase cytotoxin activates PERK, IRE1 and ATF6 endoplasmic reticulum stress-signalling pathways. *Cell Microbiol*. 2008;10(9):1775-1786.

33. Preissler S, Chambers JE, Crespillo-Casado A, et al. Physiological modulation of BiP activity by trans-protomer engagement of the interdomain linker. *eLife*. 2015;4:e08961.

34. Hu CC, Dougan SK, Winter SV, Paton AW, Paton JC, Ploegh HL. Subtilase cytotoxin cleaves newly synthesized BiP and blocks antibody secretion in B lymphocytes. *J Exp Med*. 2009;206(11):2429-2440.

35. Behnke J, Mann MJ, Scruggs F-L, Feige MJ, Hendershot LM. Members of the Hsp70 family recognize distinct types of sequences to execute ER quality control. *Mol Cell*. 2016;63(5):739-752.

36. Knarr G, Modrow S, Todd A, Gething MJ, Buchner J. BiP-binding sequences in HIV gp160. Implications for the binding specificity of bip. *J Biol Chem*. 1999;274(42):29850-29857.

37. Bush AI, Pettingell WH, Multhaup G, et al. Rapid induction of Alzheimer A beta amyloid formation by zinc. *Science*. 1994;265(5177):1464-1467.

38. Coalier KA, Paranjape GS, Karki S, Nichols MR. Stability of early-stage amyloid-β(1-42) aggregation species. *Biochim Biophys Acta*. 2013;1834(1):65-70.

39. Brumshtein B, Esswein SR, Sawaya MR, et al. Identification of two principal amyloid-driving segments in variable domains of Ig light chains in systemic light-chain amyloidosis. *J Biol Chem*. 2018;293(51):19659-19671.

40. Ferris SP, Jaber NS, Molinari M, Arvan P, Kaufman RJ. UDP-glucose:glycoprotein glucosyltransferase (UGGT1) promotes substrate solubility in the endoplasmic reticulum. *Mol Biol Cell*. 2013;24(17):2597-2608.

41. Vassilakos A, Cohen-Doyle MF, Peterson PA, Jackson MR, Williams DB. The molecular chaperone calnexin facilitates folding and assembly of class I histocompatibility molecules. *EMBO J*. 1996;15(7):1495-1506.

42. Ushioda R, Hoseki J, Araki K, Jansen G, Thomas DY, Nagata K. ERdj5 is required as a disulfide reductase for degradation of misfolded proteins in the ER. *Science*. 2008;321(5888):569-572.

43. Dong M, Bridges JP, Apsley K, Xu Y, Weaver TE. ERdj4 and ERdj5 are required for endoplasmic reticulum-associated protein degradation of misfolded surfactant protein C. *Mol Biol Cell*. 2008;19(6):2620-2630.

44. Rangarajan S, Walsh L, Lester W, et al. AAV5-factor VIII gene transfer in severe hemophilia A. *N Engl J Med*. 2017;377(26):2519-2530.

45. Rangarajan S, Kim B, Lester W, et al. Achievement of normal FVIII activity following gene transfer with valoctocogene roxaparvovec [BMN 270]: long-term efficacy and safety results in patients with severe haemophilia A [abstract]. *Haemophilia*. 2018;24(S5). Abstract T-FPMED01-001 (153).

46. Niemeyer GP, Herzog RW, Mount J, et al. Long-term correction of inhibitor-prone hemophilia B dogs treated with liver-directed AAV2-mediated factor IX gene therapy. *Blood*. 2009;113(4):797-806.

47. Nathwani AC, Reiss U, Tuddenham E, et al. Adeno-associated mediated gene transfer for hemophilia B:8 year follow up and impact of removing "empty viral particles" on safety and efficacy of gene transfer [abstract]. *Blood*. 2018;132(suppl 1):Abstract 491.

48. Kumaran V, Benten D, Follenzi A, Joseph B, Sarkar R, Gupta S. Transplantation of endothelial cells corrects the phenotype in hemophilia A mice. *J Thromb Haemost*. 2005;3(9):2022-2031.

49. Shahani T, Covens K, Lavend'homme R, et al. Human liver sinusoidal endothelial cells but not hepatocytes contain factor VIII. *J Thromb Haemost*. 2014;12(1):36-42.

50. Everett LA, Cleuren AC, Khoriaty RN, Ginsburg D. Murine coagulation factor VIII is synthesized in endothelial cells. *Blood*. 2014;123(24):3697-3705.

51. Zolotukhin I, Markusic DM, Palaschak B, Hoffman BE, Srikanthan MA, Herzog RW. Potential for cellular stress response to hepatic

factor VIII expression from AAV vector. *Mol Ther Methods Clin Dev*. 2016;3:16063.

52. Lange AM, Altynova ES, Nguyen GN, Sabatino DE. Overexpression of factor VIII after AAV delivery is transiently associated with cellular stress in hemophilia A mice. *Mol Ther Methods Clin Dev*. 2016;3:16064.

53. Nakagawa H, Umemura A, Taniguchi K, et al. ER stress cooperates with hypernutrition to trigger TNF-dependent spontaneous HCC development. *Cancer Cell*. 2014;26(3):331-343.

54. Jenkins PV, Rawley O, Smith OP, O'Donnell JS. Elevated factor VIII levels and risk of venous thrombosis. *Br J Haematol*. 2012;157(6):653-663.

55. Kyrle PA, Minar E, Hirschl M, et al. High plasma levels of factor VIII and the risk of recurrent venous thromboembolism. *N Engl J Med*. 2000;343(7):457-462.

56. Liu Q, Yang J, Zong Y, Columbus L, Zhou L. 6ASY: BiP-ATP2. RCSB Protein Data Bank (PDB). https://www.rcsb.org/structure/6ASY. Accessed 11 January 2019.

57. Assenza S, Sassi AS, Kellner R, Schuler B, De Los Rios P, Barducci A. Efficient conversion of chemical energy into mechanical work by Hsp70 chaperones. *eLife*. 2019;8:e48491.